Monthly Notices
of the
ROYAL ASTRONOMICAL SOCIETY

MNRAS **440,** 2616–2624 (2014) doi:10.1093/mnras/stu426

Chemistry and radiative transfer of water in cold, dense clouds

Eric Keto,[1]★ Jonathan Rawlings[2]★ and Paola Caselli[3]★

[1]*Harvard–Smithsonian Center for Astrophysics, 160 Garden St, Cambridge, MA 02420, USA*
[2]*University College London, London, UK*
[3]*School of Physics and Astronomy, University of Leeds, Leeds LS2 9JT, UK*

Accepted 2014 March 3. Received 2014 March 1; in original form 2013 December 19

ABSTRACT

The *Herschel Space Observatory*'s recent detections of water vapour in the cold, dense cloud L1544 allow a direct comparison between observations and chemical models for oxygen species in conditions just before star formation. We explain a chemical model for gas-phase water, simplified for the limited number of reactions or processes that are active in extreme cold (<15 K). In this model, water is removed from the gas phase by freezing on to grains and by photodissociation. Water is formed as ice on the surface of dust grains from O and OH and released into the gas phase by photodesorption. The reactions are fast enough with respect to the slow dynamical evolution of L1544 that the gas-phase water is in equilibrium for the local conditions throughout the cloud. We explain the paradoxical radiative transfer of the H_2O ($1_{10}-1_{01}$) line. Despite discouragingly high optical depth caused by the large Einstein A coefficient, the subcritical excitation in the cold, rarefied H_2 causes the line brightness to scale linearly with column density. Thus, the water line can provide information on the chemical and dynamical processes in the darkest region in the centre of a cold, dense cloud. The inverse P-Cygni profile of the observed water line generally indicates a contracting cloud. This profile is reproduced with a dynamical model of slow contraction from unstable quasi-static hydrodynamic equilibrium (an unstable Bonnor–Ebert sphere).

Key words: astrochemistry – radiative transfer – ISM: abundances – ISM: individual objects: L1544 – ISM: molecules.

1 INTRODUCTION

Observations of water vapor in the interstellar medium (ISM) by the *Infrared Space Observatory* (van Dishoeck et al. 1999) and the *Submillimeter Wave Astronomy Satellite* (*SWAS*; Bergin et al. 2000) show general agreement with chemical models for warm (>300 K) conditions in the ISM (Melnick et al. 2000; Neufeld et al. 2000). However, in cold conditions, most of the water is frozen on to dust grains (Viti et al. 2001; van Dishoeck, Herbst & Neufeld 2013), and the production of water occurs mainly on the grain surfaces. In order to test chemical models that include grain-surface chemistry, we used the Heterodyne Instrument for the Far-Infrared (HIFI; de Graauw et al. 2010) on the *Herschel Space Observatory* to observe the H_2O ($1_{10}-1_{01}$) line in the cold, dense cloud L1544 (Caselli et al. 2010, 2012). The first of these two *Herschel* observations was made with the wide-band spectrometer (WBS) and detected water vapour in absorption against the weak continuum radiation of dust in the cloud. Follow-up observations with higher spectral resolution and sensitivity, made with the high-resolution spectrometer, confirmed the absorption and detected a blueshifted emission line that was predicted by theoretical modelling (Caselli et al. 2010), but too narrow to be seen by the WBS in the first observation.

With the better constraints provided by the second observation, we improved the chemical and radiative transfer modelling in our previous papers. We modified the radiative transfer code MOLLIE to calculate the line emission in the approximation that the molecule is subcritically excited. This assumes that the collision rate is so slow that every excitation leads immediately to a radiative de-excitation and the production of one photon which escapes the cloud, possibly after many absorptions and re-emissions, before another excitation. The emission behaves as if the line were optically thin with the line brightness proportional to the column density. This approximation can be correct even at very high optical depth as long as the excitation rate is slow enough, $C < A/\tau$, where C is the collision rate, A is the spontaneous emission rate, and τ the optical depth (Linke et al. 1977). Caselli et al. (2012) presented the observations and the results of this modelling.

In this paper, we discuss in detail the theory behind the modelling. A comparison of the spectral line observation with theory requires three models. First, we require a hydrodynamical model to

★ E-mail: keto@cfa.harvard.edu (EK); jcr@star.ucl.ac.uk (JR); p.caselli@leeds.ac.uk (PC)

describe the density, velocity, and temperature across the cloud. We use a model of slow contraction in quasi-static unstable equilibrium that we developed in our previous research (Keto & Field 2005; Keto & Caselli 2010). Secondly, we require a chemical model to predict the molecular abundance across the varying conditions in the cloud. Following the philosophy for simplified chemical networks in Keto & Caselli (2008) or Bethell & Bergin (2009), we extract from a general chemical model for photodissociation regions (PDR; Hollenbach et al. 2009) a subset of reactions expected to be active in cold conditions, principally grain-surface reactions as well as freeze-out and photodissociation. Thirdly, we require a radiative transfer model to generate a simulated molecular line. We modify our non-local thermodynamic equilibrium (LTE) radiative transfer code MOLLIE to use the escape probability approximation. This allows better control of the solution in extreme optical depth.

The three models are described in more detail in three sections below. The relevant equations are included in the appendices.

2 THE THREE MODELS

2.1 The cold, dense clouds

Given their importance as the nurseries of star formation, the small (<0.5 pc), cold (<15 K), dense ($n > 10^3$ cm^{-3}) clouds in low-mass star (<2 M$_\odot$) forming regions such as Taurus are widely studied (Bergin & Tafalla 2007; di Francesco et al. 2007). Observations show a unique simplicity. They contain no internal sources of heat, stars, or protostars. Their internal turbulence is subsonic, barely broadening their molecular line widths above thermal (Myers & Benson 1983). With most of their internal energy in simple thermal energy, and the weak turbulence just a perturbation (Keto et al. 2006; Broderick & Keto 2010), the observed density structure approximates the solution of the Lane–Emden equation for hydrostatic equilibrium (Lada et al. 2003; Kandori et al. 2005). Correspondingly, most are nearly spherical with an average aspect ratio of about 1.5 (Jijina, Myers & Adams 1999). They are heated from the outside both by cosmic rays and by the ultraviolet (UV) background of starlight and are cooled from the inside by long wavelength molecular line and dust continuum radiation (Evans et al. 2001). Because of their simplicity, we understand the structure and dynamics of these small, cold, dense clouds better than any other molecular clouds in the ISM. They are therefore uniquely useful as a laboratory for testing hypotheses of more complex phenomena such as the chemistry of molecular gas.

2.2 Structure and dynamics

Our physical model for cold, dense clouds is computed with a spherical Lagrangian hydrodynamic code with the gas temperature set by radiative equilibrium between heating by external starlight and cosmic rays and cooling by molecular line and dust radiation. The theory is discussed in Keto & Field (2005) and Keto & Caselli (2008).

In our previous research (Keto & Caselli 2010), we generated a dynamical model for the particular case of L1544 by comparing observations and snapshots in time out of a theoretical model for the contraction towards star formation. We began the hydrodynamic evolution with a 10 M$_\odot$ Bonnor–Ebert (BE) sphere with a central density of 10^4 cm^{-3} in unstable dynamical equilibrium and in radiative equilibrium with an external UV field of one Habing flux. In the early stages of contraction, the cloud evolves most rapidly in the centre. As long as the velocities remain subsonic, the evolving density profile closely follows a sequence of spherical equilibria or BE spheres with increasing central densities. We compared modelled CO and N_2H^+ spectra during the contraction against those observed in L1544 and determined that the stage of contraction that best matches the data has a central density of 1×10^7 cm^{-3} and a maximum inward velocity just about the sound speed (Keto & Caselli 2010). Fig. 1 shows the density and velocity at this time along with the H_2O abundance and temperature.

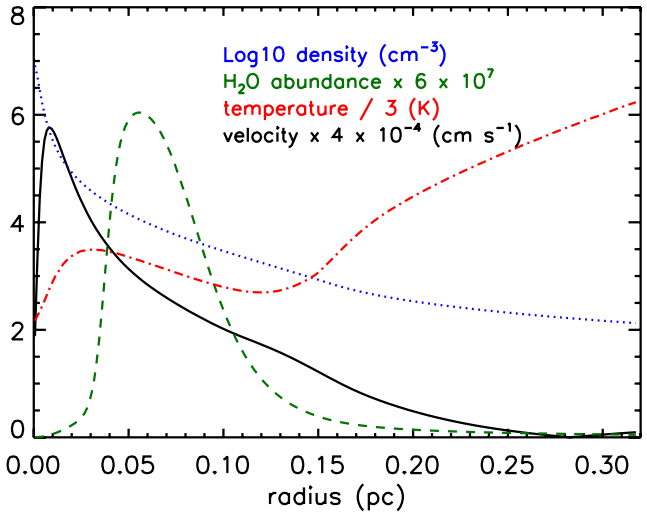

Figure 1. Model of a slowly contracting cloud in quasi-static unstable equilibrium. The log of the density profile in cm^{-3} is shown in blue (dotted line), the fractional abundance of H_2O with respect to H_2 is shown in green (dashed line), the velocity as the black (solid) line, and the gas temperature as the red (dot–dashed) line. The model spectrum is shown in Fig. 8.

In the present investigation, we modify our numerical hydrodynamic code to include cooling by atomic oxygen. This improves the accuracy of the calculated gas temperature in the PDR outside the molecular cloud. The equations governing the cooling by the fine structure lines of atomic oxygen are presented in the appendix.

2.3 Chemistry of H_2O in cold conditions

The cold conditions in L1544 allow us to simplify the chemical model for gas-phase water. We include the four oxygen-bearing species most abundant in cold, dark clouds, O, OH, H_2O gas, and H_2O ice. Even though all three gas-phase molecules may freeze on to the grains, we consider only one species of ice because the formation of water from OH and the formation of OH from O are rapid enough on the grain surface that most of the ice is in the form of H_2O. To provide a back reaction for the freeze-out of atomic oxygen and preserve detailed balance, we arbitrarily assign a desorption rate for atomic O equal to that of H_2O even though the production of atomic O from H_2O ice is not indicated. Our simplified model is shown in Fig. 2. The resulting abundances, calculated as equilibria between creation and destruction, are shown in Figs 3 and 4. Fig. 3 shows the abundances near the PDR boundary as a function of the visual extinction, A_V. Fig. 4 shows the abundances against the log of the radius to emphasize the centre.

Gas-phase water is created by UV photodesorption of water ice which also creates gas-phase OH in a ratio $H_2O/OH = 2$ (Hollenbach et al. 2009). In the outer part of the cloud, the UV radiation derives from the background field of external starlight. The inward attenuation of the UV flux is modelled from the visual extinction as $\exp(-1.8A_V)$. In the interior where all the external UV radiation

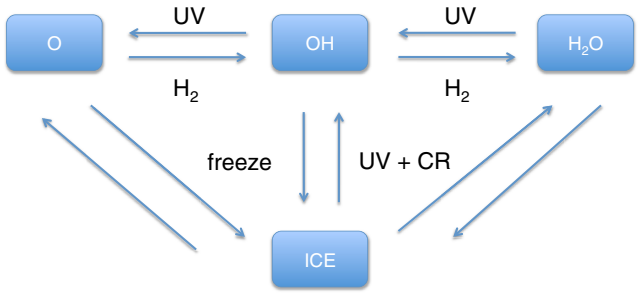

Figure 2. Simplified model of the oxygen chemistry in a cold cloud. The model includes three gas-phase species and H_2O ice. The significant reactions at cold temperatures (T < 300 K) are the freeze-out of molecules colliding with dust grains, cosmic ray, photodesorption of the ice, and photodissociation of the gas-phase molecules.

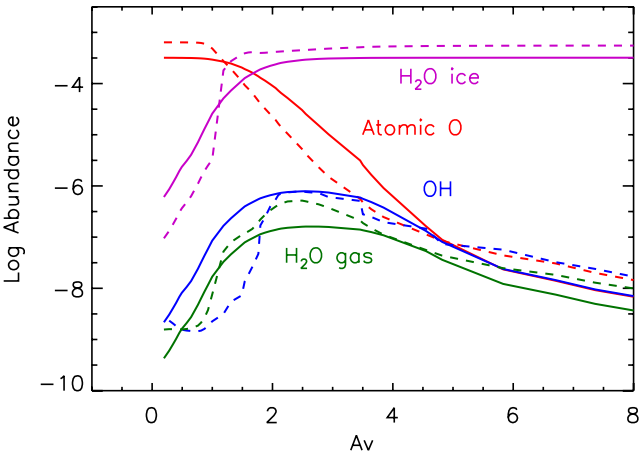

Figure 3. Abundances of oxygen species as a function of A_V for the model of L1544 based on a slowly contracting BE sphere. The figure emphasizes the variation of abundances in the PDR at the edge. The figure compares the abundances for the physical conditions in (Fig. 1) from two models: Hollenbach et al. (2009, dashed lines; courtesy E. Bergin) and our simplified model (Fig. 2). Fig. 4 shows abundances from the same models but plotted against log radius to emphasize the variations in the centre.

has been attenuated, the only UV radiation is generated by cosmic ray strikes on H_2. In our previous paper (Caselli et al. 2012), we set this secondary UV radiation to 1×10^{-3} times the Habing flux ($G_0 = 1$; Hollenbach et al. 2009). In our current model, we use a lower level, 1×10^{-4}, that is more consistent with estimated rates (Shen et al. 2004). The difference in abundance for the two rates is shown in Fig. 4.

H_2O and OH are removed from the gas phase by UV photodissociation and by freezing on to dust grains. To preserve detailed balance with the photodissociation, we include the back reactions, the gas-phase production of H_2O, $O + H_2 \rightarrow OH$, and $OH + H_2 \rightarrow H_2O$, even though these are not expected to be important in cold gas. Removal of gas-phase water by freeze-out is important in the interior where the higher gas density increases the dust–gas collision rate and hence the freeze-out rate.

We assume that the gas-phase ion–neutral reactions that lead to the production of water are less important at cold temperatures (<15 K) than the reactions that produce water on the surfaces of ice-coated dust grains. Thus, we do not include gas-phase ion–neutral reactions in the model. This is valid if the oxygen is quickly

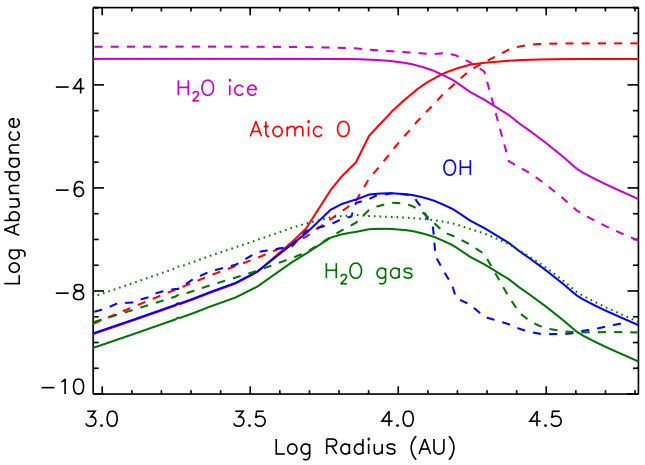

Figure 4. Abundances of oxygen species, same as Fig. 3, except plotted against the log of the radius rather than visual extinction. This figure emphasizes the variations in abundance in the centre. The figure shows the H_2O abundance calculated with our simplified model using two values for the cosmic ray-induced UV photodesorption (equation B13). The solid green line shows the abundance calculated with factor $\alpha = 10^{-4}$. The dotted line shows the abundance calculated with factor $\alpha = 10^{-3}$. The abundance calculated with the Hollenbach et al. (2009) model assumes $\alpha = 10^{-3}$ (dashed line).

removed from the gas phase by freeze-out and efficiently converted into water ice on the grain surface.

By leaving out CO, we avoid coupling in the carbon chemistry. Although we already have a simple model for the carbon chemistry (Keto & Caselli 2008, 2010), we prefer to keep our oxygen model as simple as possible. This could create an error of a factor of a few in the abundance of the oxygen species. Carbon is one-third as abundant as oxygen, and in certain conditions CO is the dominant carbon molecule. Therefore, as much as one-third of the oxygen could potentially be bound in CO. Ignoring O_2 is less of a problem. Created primarily by the reaction of OH with atomic oxygen, O_2 tends to closely follow the abundance of OH. Since the amount of oxygen in OH should be 1 per cent or less (Fig. 3), the abundance of O_2 does not affect the abundances of the other oxygen species, O, OH, and H_2O.

Figs 3 and 4 compare the abundances from our simplified network with those from the more complex network of Hollenbach et al. (2009; courtesy of E. Bergin) that includes gas-phase neutral–neutral and ion–neutral reactions. In this calculation, we hold the cloud at the same time in its dynamical evolution and allow the chemistry to evolve for 10 Myr from the assumed starting conditions in which all species are atomic and neutral. Both models generally agree. The gas-phase water peaks in a region near the boundary. Here, there is enough external UV to rapidly desorb the water from the ice, but not so much as to dissociate all the molecules. Further inwards, the abundance of water falls as the gas density and the dust–gas collision rate (freeze-out rate) both increase while the photodesorption rate decreases with the attenuation of the UV radiation. At high A_V, the water is desorbed only by cosmic rays and the UV radiation they produce in collisions with H_2. The general agreement between the two models suggests that the simple model includes the processes that are significant in the cold environment. The rate equations for the processes selected for the simplified model are listed in Appendix B.

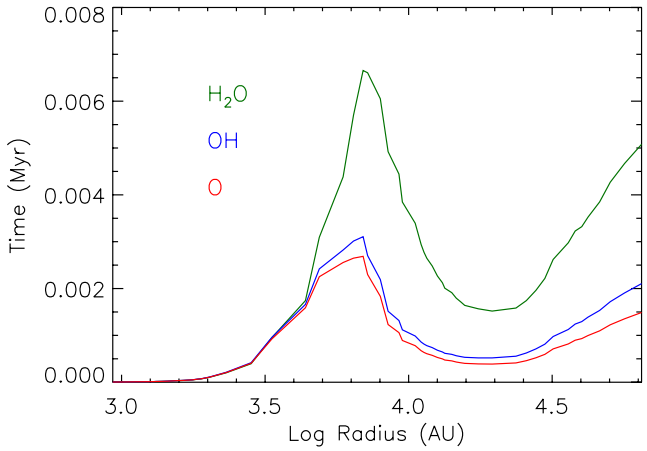

Figure 5. Time-scales for chemical equilibrium. From top to bottom, the three lines show the equilibration time-scales for H_2O, OH, and O calculated from equation (1) and the reaction rates in the appendix.

Our simple model calculates equilibrium abundances. We can estimate the equilibrium time-scale from the combined rates for creation and destruction (Caselli et al. 2002) as

$$t = \frac{t_{\rm creation} t_{\rm destruction}}{t_{\rm creation} + t_{\rm destruction}}, \quad (1)$$

where the time-scales are the inverses of the rates. Fig. 5 shows the equilibrium time-scales for each species as a function of radius. These may be compared with the time for the hydrodynamic evolution. A cloud with a mass of 10 $M_\odot$ and a central density of 2×10^6 cm^{-3} has a free-fall time, $t_{\rm ff} = 0.03$ Myr, using the central density in the standard equation whereas the sound crossing time is about 2 Myr (Keto & Caselli 2010). Because the chemical time-scales are all shorter than the dynamical time-scales, the chemistry reaches equilibrium before the conditions, density, temperature, and UV flux change.

In this estimate of the time-scale for chemical evolution, we are asking whether the oxygen chemistry in the contracting molecular cloud can maintain equilibrium as the cloud evolves dynamically. This is different from the question of how long it would take for the chemistry to equilibrate if the gas were held at molecular conditions but evolving from an atomic state.

2.4 Radiative transfer

We use our radiative transfer code MOLLIE (Keto 1990; Keto & Rybicki 2010) to compute model H_2O spectra to compare with the *Herschel* observation. Here, we encounter an interesting question. The large Einstein A coefficient of the H_2O ($1_{10}-1_{01}$) line results in optical depths across the cloud of several hundreds to a thousand depending on excitation. High optical depths generally result in radiative trapping and enhanced excitation of the line. In this case, the line brightness could have a non-linear relationship to the column density. For example, the line could be saturated. On the other hand, the large Einstein A means that the critical density for collisional de-excitation is quite high (1×10^8 cm^{-3}) at the temperatures, <15 K, higher than the maximum density (1×10^7 cm^{-3}) in our dynamical model of L1544. This suggests that the line emission should be proportional to the column density.

This question was addressed by Linke et al. (1977) who proposed a solution using the escape probability approximation (Kalkofen 1984). They assumed a two-level molecule, equal statistical weights in both levels, and the mean radiation field, $\bar{J}$, set by the escape probability, β, as

$$\bar{J} = J_0\beta + (1-\beta)S, \quad (2)$$

where J_0 is the continuum from dust and the cosmic microwave background, S is the line source function, and

$$\beta = (1 - \exp(-\tau))/\tau. \quad (3)$$

After a satisfying bout with three pages of elementary algebra and some further minor approximations, they show that as long as $C < A/\tau$, the line brightness is linearly dependent on the column density, no matter whether the optical depth is low or high, provided that the line is not too bright.

To determine whether the water emission line brightness in L1544 has a non-linear or linear dependence, we numerically solve the equations for the two-level molecule with no approximations other than the escape probability and plot the result. Figs 6 and 7 show the dependence of the antenna temperature on the density for low and

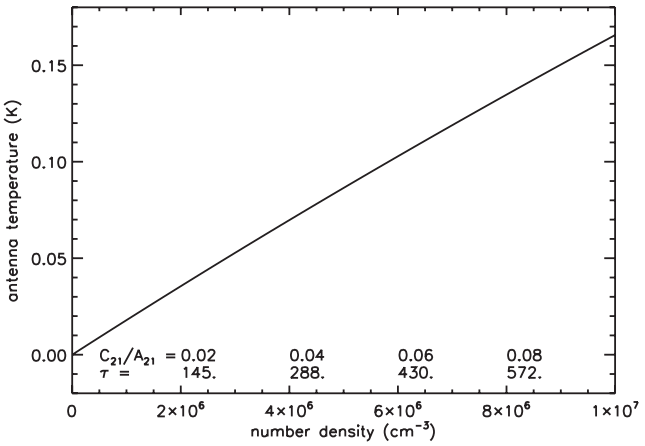

Figure 6. The dependence of the observed antenna temperature of the H_2O ($1_{10}-1_{01}$) line on the H_2 number density (cm^{-3}). Because the optical depth and the ratio of the collision rate to spontaneous emission rate (C/A) are both linearly dependent on the density, the abscissa can be labelled in these units as well. Both are shown above the axis. The antenna temperature is linearly dependent on the density or column density even at very high optical depth as long as the ratio C/A is small.

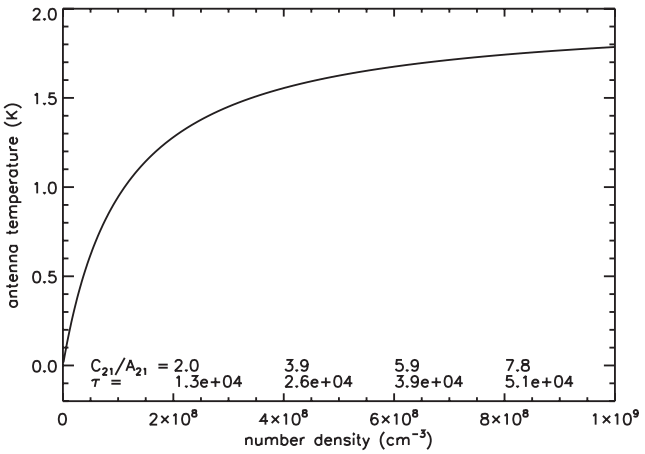

Figure 7. The dependence of the observed antenna temperature of the H_2O line ($1_{10}-1_{01}$) on the number density. Same as Fig. 6 but at higher densities where the ratio C/A is no longer small and the dependence of the antenna temperature on the density is no longer linear.

high densities, respectively. Since the column density, the optical depth, and the ratio *C*/*A* are all linearly dependent on the density, any of these may be used on the abscissa. The latter two are shown just above the axis. Fig. 6 shows that the antenna temperature of the water line emission is linearly dependent on the column density even at high density or high optical depth. Fig. 7 shows that the linear relation breaks down when *C*/*A* is no longer small. The densities in both figures show that the water line emission in L1544 is in the linear regime.

For an intuitive explanation, suppose that a photon is absorbed on average once per optical depth of one. A photon may be absorbed and another re-emitted many times in escaping a cloud of high optical depth. The time-scale for each de-excitation is A^{-1}. Therefore, the time that it takes a photon to escape the cloud is τ/A. As long as this time is shorter than the collisional excitation time $(1/C)$, then on average, an emitted photon will escape the cloud before another photon is created by the next collisional excitation event and radiative de-excitation. In this case, the line remains subcritically excited. The molecules are in the lower state almost all the time. This is the same condition that would prevail if the cloud were optically thin ($\bar{J} = 0$ or $\beta = 1$). On this basis, in our earlier paper, we determined the emissivity and opacity of the H_2O line in L1544 by setting $\bar{J} = 0$ (Caselli et al. 2012). This approximation was earlier adopted in analysing water emission observed by *SWAS* (Snell et al. 2000) where it is referred to as 'effectively optically thin'.

In this current paper, we seek an improved estimate of $\bar{J} > 0$ and $\beta < 1$ by using the escape probability formalism as suggested by Linke et al. (1977). We determine β using the local velocity gradient as given by our hydrodynamical model along with the local opacity using the Sobolev or large velocity gradient (LVG) approximation (equations 3–40; Kalkofen 1984). We use the six-ray approximation for the angle averaging. We allow for one free scaling parameter on β to match the modelled emission line brightness to the observation. We scale the LVG opacity by 1/2. Because the opacity, column density, and line brightness are all linearly related, the scaling could be considered to derive from any or any combination of these parameters. Given all the uncertain parameters, for example, the mean grain cross-section which also affects the line brightness (Appendix B), this factor of 2 is not significant.

An alternative method to calculate the excitation is the accelerated Λ-iteration algorithm. We do not know if this method is reliable with the extremely high optical depth, several hundreds to a thousand. Λ-iteration generally converges, but whether it converges to the correct solution cannot be determined from the algorithm itself (equations 6–33; Mihalas 1978).

The excitation may be uncertain, but analysis with the escape probability method allows us to understand the effect of the uncertainty. For example, because we know that the dependence of the line brightness on the opacity or optical depth is linear, we can say that any uncertainty in excitation results in the same percentage uncertainty in the abundance of the chemical model or the pathlength of the structural model.

Once $\bar{J}$ is determined everywhere in the cloud, the equations of statistical equilibrium are solved to determine the emissivity and opacity. These are then used in the radiative transfer equation to produce the simulated spectral line emission and absorption. This calculation is done in MOLLIE in the same way as if $\bar{J}$ were determined by any other means, for example, by Λ-iteration.

Both the emissivity and the opacity depend on frequency through the Doppler-shifted line profile function (equation 2.14; Kalkofen 1984) that varies as a function of position in the cloud. We use a line profile function that is the thermal width plus a microturbulent Gaussian broadening of 0.08 km s^{-1} derived from our CO modelling (Keto & Caselli 2010). By the approximation of complete frequency redistribution (equations 10–39; Mihalas 1978), both have the same frequency dependence. This also implies that each photon emitted after an absorption event has no memory of the frequency of the absorbed photon. It is emitted with the frequency probability distribution described by the line profile function Doppler shifted by the local velocity along the direction of emission. We also assume complete redistribution in angle.

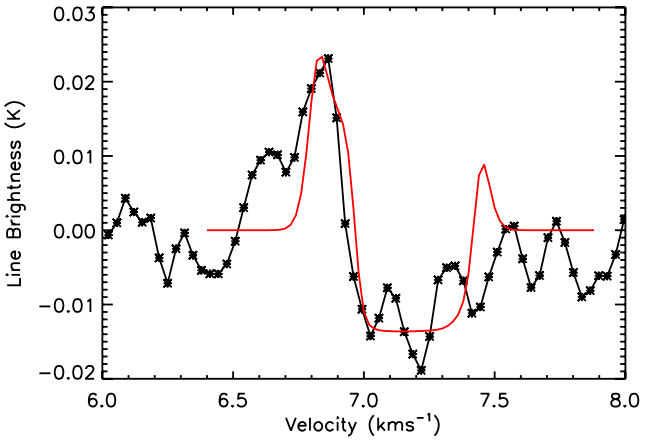

Figure 8. Observed spectrum of H_2O ($1_{10}-1_{01}$) (black lines with crosses) compared with modelled spectrum (simple red line) for slow contraction at the time that the central density reaches 1×10^7 cm^{-3}. The model structure is shown in Fig. 1.

Fig. 8 shows the modelled line profile against the observed profile. The V_{LSR} is assumed to be 7.16 km s^{-1}, slightly different than 7.2 km s^{-1} used in Caselli et al. (2012). The lower value is chosen here as the best fit to the H_2O observation.

The combination of blueshifted emission and redshifted absorption is the inverse P-Cygni profile characteristic of contraction, with the emission and absorption split by the inward gas motion in the front and rear of the cloud. The absorption against the dust continuum is unambiguously from the front side indicating contraction rather than expansion. This profile has also been seen in other molecules in other low-mass cold, dense clouds, with the absorption against the dust continuum (Di Francesco et al. 2001).

In L1544, because the inward velocities are below the sound speed, and the H_2O line width is just larger than thermal, the emission is shifted with respect to the absorption by less than a line width. In the observations, what appears to be a blueshifted emission line is just the blue shoulder and wing of the complete emission, most of which is brighter, redder and wider than the observed emission.

Our model also shows weaker emission to the red of the absorption line. This emission is from inward moving gas in the front side of the contracting zone. Again most of the emission is absorbed by the envelope and only the blue shoulder of the line is seen. The asymmetry between the red and blue emission comes about because the absorbing envelope, which is on the front side of the cloud, is closer in velocity to inward flowing gas (red) on the front side of the contraction. This is the same effect that produces the blue asymmetric or double-peaked line profiles seen in contraction in molecular lines without such significant envelope absorption (Anglada et al. 1987). The model shows more red emission than is seen in the observations. This red emission may be absorbed by foreground gas that is not in the model. Fig. 1 of Caselli et al. (2012) shows

additional redshifted absorption in H_2O and redshifted emission in CO, both centred around 9 km s^{-1}. The blue wing of this redshifted water line may be absorbing the red wing of the emission from the dense cloud.

If L1544 were static, no inward contraction, the emission from the centre would be at the same frequency as the envelope. Because of the extremely high optical depth, the absorption line is saturated and would absorb all the emission. We would see only the absorption line. The depth of the absorption line is set by brightness of the dust continuum which is weak (0.011 K) and not by the optical depth of the line which is high (few hundreds to a thousand).

In the current radiative transfer calculation, we also use a slightly different collisional excitation rate than before. The collisional rates for ortho-H_2O are different with ortho- and para-H_2. In our previous paper (Caselli et al. 2012), we modelled the H_2 ortho-to-para ratio as a lower limit 1:1 or higher. Here, we assume that almost all the hydrogen, 99.9 per cent, is in the para state. This is suggested by recent chemical models that require a low ortho-to-para ratio to produce the high deuterium fraction observed in cold, dense clouds (e.g. Kong et al. 2013; Sipilä, Caselli & Harju 2013).

3 INTERPRETATION

The shape of the line profile (Fig. 8) is unaffected by any uncertainty in the excitation which scales the emission across the spectrum. The absorption is saturated and does not scale with the excitation. Because of the very high critical density for collisional de-excitation, we know that the line emission is generated only in the densest gas ($>10^6$ cm^{-3}) within a few thousand au of the centre. Thus, the observation of the inverse P-Cygni profile seen in H_2O confirms the model for quasi-hydrostatic contraction with the highest velocities near the centre (Fig. 1).

The chemical model requires external UV to create the gas-phase water by photodesorption. This confirms the physical model of L1544 as a molecular cloud bounded by a PDR. The UV flux necessarily creates a higher temperature, up to about 100 K at the boundary by photoelectric heating. This helps maintain the pressure balance at the boundary consistent with the model of a BE sphere.

4 UNCERTAINTIES

The comparison of the simulated and observed spectral line involves three models each with multiple parameters. Unavoidably, the choice of parameters in any one of the three models affects not only the choice of other parameters in the other two models but also the interpretation. It would be a mistake to focus on the uncertainties in any one of the models to the exclusion of the others. For example, because of the linear relationship between the line brightness, the optical depth, and the opacity, uncertainties in the excitation, pathlength, and abundance have equal effect on the spectrum. A factor of 2 uncertainty in the excitation can be compensated by a factor of 2 in the pathlength or a factor of 2 in the abundance of H_2O. The pathlength is unknown. On the plane of the sky, L1544 has an axial ratio of 2:1, but we are using a spherical model for the cloud. Our rates in the chemical model involve estimation of the surface density of sites for desorption and the covering fraction of water ice on the grains. The latter is assumed to be one even though we know that CO and methane ice, not included in the simple model, make up a significant fraction of the ice mantle. The radiative excitation, parametrized as β in the escape probability is also uncertain because of the competing effects of high optical depth and subcritical excitation.

On a linear plot, a factor of 2 difference in the brightness of the simulated and observed spectral line looks to be a damning discrepancy. However, there is at least this much uncertainty in each of the three models and this does not significantly affect the conclusions of the study, namely that the cloud can be modelled as a slowly contracting BE sphere bounded by a PDR with the gas-phase water abundance set by grain-surface reactions.

In this paper, we concentrate on the observation of H_2O, but there are also other constraints that define the model. These are both observational and theoretical. In an earlier paper, we showed how observations of CO and N_2H^+ define the physical model with the two spectral lines giving us information on the outer and inner regions of the cloud, respectively. In this regard, the water emission gives us information in the central few thousand au of the cloud where the density approaches or exceeds the critical density for de-excitation. This small volume of rapid inflow and high density does not much affect the N_2H^+ spectrum which is generated in a much larger volume and has no affect at all on the CO spectrum. A successful model for L1544 has to satisfy the constraints of all the data. On the theoretical side, there is an infinite space of combinations of abundance, density, velocity, and temperature that would form models that match the data. Only models that are physically motivated are of interest. It may be tempting to change the abundances, velocities, or densities arbitrarily, but this is unlikely to be a useful exercise giving the infinite possibilities. A successful model for L1544 has to be relevant to plausible theory.

There is a natural prejudice for more complex models that in principle contain more details. The goal of our simplified models is to enhance our understanding of the most significant phenomena. In our research on cold, dense clouds, spanning a number of papers, we have developed simplified models for the density and temperature structure, for the dynamics including oscillations, for the CO chemistry, and in this paper, for H_2O chemistry and radiative transfer. Each of these models isolates one or a few key physical processes and shows how they generate the observables and operate to control the evolution towards star formation.

5 CONCLUSIONS

A simplified chemical model for cold oxygen chemistry primarily by grain-surface reactions is verified by comparing the simulated spectrum of the H_2O ($1_{10}-1_{01}$) line against an observation of water vapour in L1544 made with HIFI spectrometer on the *Herschel Space Observatory*.

This model reproduces the observed spectrum of H_2O, and also approximates the abundances calculated by a more complete model that includes gas-phase neutral–neutral and ion–neutral reactions.

The gas-phase water is released from ice grains by UV photodesorption. The UV radiation derives from two sources: external starlight and collisions of cosmic rays with molecular hydrogen. The latter may be important deep inside the cloud where the visual extinction is high enough (>50 mag) to block out the external UV radiation.

Water is removed from the gas phase by photodissociation and freeze-out on to grains. The former is important at the boundary where the UV from external starlight is intense enough to create a PDR. Here, atomic oxygen replaces water as the most abundant oxygen species. In the centre where the external UV radiation is completely attenuated, freeze-out is the significant loss mechanism.

Time-dependent chemistry is not required to match the observations because the time-scale for the chemical processes is short compared to the dynamical time-scale.

The molecular cloud L1544 is bounded by a PDR.

The water emission derives only from the central few thousand au where the gas density approaches the critical density for collisional de-excitation of the water line. In the model of hydrostatic equilibrium, the gas density in the centre is rising with decreasing radius more steeply than the abundance of water is decreasing by freeze-out. Thus, the water spectrum provides unique information on the dynamics in the very centre.

The large Einstein A coefficient (3×10^{-3} s^{-1}) of the 557 GHz H_2O ($1_{10}-1_{01}$) line results in extremely high optical depth, several hundreds to a thousand. However, the density ($<10^7$ cm^{-3}) and temperature (<15 K) are low enough that the line is subcritically excited. The result is that the line brightness under these conditions is directly proportional to the column density.

ACKNOWLEDGEMENTS

The authors acknowledge Simon Bruderer, Fabien Daniel, Michiel Hogerheijde, Joe Mottram and Floris van der Tak for interesting discussions on the radiative transfer of water. PC acknowledges the financial support of the European Research Council (ERC; project PALs 320620) and the successive rolling grants awarded by the UK Science and Technology Funding Council. JR acknowledges the financial support of the Submillimeter Array Telescope.

REFERENCES

Anglada G., Rodriguez L. F., Canto J., Estalella R., Lopez R., 1987, A&A, 186, 280
Bergin E. A., Tafalla M., 2007, ARA&A, 45, 339
Bergin E. A. et al., 2000, ApJ, 539, L129
Bethell T., Bergin E., 2009, Science, 326, 1675
Broderick A. E., Keto E., 2010, ApJ, 721, 493
Caselli P., Walmsley C. M., Zucconi A., Tafalla M., Dore L., Myers P. C., 2002, ApJ, 565, 344
Caselli P. et al., 2010, A&A, 521, L29
Caselli P. et al., 2012, ApJ, 759, L37
Conrath B. J., Gierasch P. J., 1984, Icarus, 57, 184
de Graauw T. et al., 2010, A&A, 518, L6
Di Francesco J., Myers P. C., Wilner D. J., Ohashi N., Mardones D., 2001, ApJ, 562, 770
di Francesco J., Evans N. J., II, Caselli P., Myers P. C., Shirley Y., Aikawa Y., Tafalla M., 2007, in Reipurth B., Jewitt D., Keil K., eds, Protostars and Planets V. Univ. Arizona Press, Tuscon, p. 17
Evans N. J., II, Rawlings J. M. C., Shirley Y. L., Mundy L. G., 2001, ApJ, 557, 193
Fouchet T., Lellouch E., Feuchtgruber H., 2003, Icarus, 161, 127
Habing H. J., 1968, Bull. Astron. Inst. Neth., 19, 421
Hollenbach D., Kaufman M. J., Bergin E. A., Melnick G. J., 2009, ApJ, 690, 1497
Jijina J., Myers P. C., Adams F. C., 1999, ApJS, 125, 161
Kalkofen W., 1984, Methods in Radiative Transfer. Cambridge Univ. Press, Cambridge
Kandori R. et al., 2005, AJ, 130, 2166
Keto E. R., 1990, ApJ, 355, 190
Keto E., Caselli P., 2008, ApJ, 683, 238
Keto E., Caselli P., 2010, MNRAS, 402, 1625
Keto E., Field G., 2005, ApJ, 635, 1151
Keto E., Rybicki G., 2010, ApJ, 716, 1315
Keto E., Broderick A. E., Lada C. J., Narayan R., 2006, ApJ, 652, 1366
Kong S., Caselli P., Tan J. C., Wakelam V., 2013, preprint (arXiv:1312.0971)
Lada C. J., Bergin E. A., Alves J. F., Huard T. L., 2003, ApJ, 586, 286
Linke R. A., Goldsmith P. F., Wannier P. G., Wilson R. W., Penzias A. A., 1977, ApJ, 214, 50
Mathis J. S., Rumpl W., Nordsieck K. H., 1977, ApJ, 217, 425
Melnick G. J. et al., 2000, ApJ, 539, L87
Mihalas D., 1978, Stellar Atmospheres, 2nd edn. Freeman & Co., San Francisco
Myers P. C., Benson P. J., 1983, ApJ, 266, 309
Neufeld D. A. et al., 2000, ApJ, 539, L107
Rawlings J. M. C., Hartquist T. W., Menten K. M., Williams D. A., 1992, MNRAS, 255, 471
Shen C. J., Greenberg J. M., Schutte W. A., van Dishoeck E. F., 2004, A&A, 415, 203
Sipilä O., Caselli P., Harju J., 2013, A&A, 554, A92
Snell R. L. et al., 2000, ApJ, 539, L101
Tielens A. G. G. M., 2005, The Physics and Chemistry of the Interstellar Medium. Cambridge Univ. Press, Cambridge
Tielens A. G. G. M., Hollenbach D., 1985, ApJ, 291, 722
van Dishoeck E. F. et al., 1999, in Cox P., Kessler M., eds, ESA SP-427: The Universe as Seen by ISO. ESA, Noordwijk, p. 437
van Dishoeck E. F., Herbst E., Neufeld D. A., 2013, Chem. Rev., 113, 9043
Viti S., Roueff E., Hartquist T. W., Pineau des Forêts G., Williams D. A., 2001, A&A, 370, 557

APPENDIX A: COOLING BY ATOMIC OXYGEN FINE STRUCTURE LINES

The fine structures lines of C^+ and atomic O are the major coolants in the diffuse ($n < 1000$ cm^{-3}), photodissociated gas around the molecular clouds. The more important coolant at temperatures less than 100 K is C^+. At higher temperatures, oxygen becomes increasingly important in the energy balance. The reason is that the 63.2 and 145.6 μm fine structure lines of atomic oxygen have upper states $^3P_1$ and $^3P_0$ that are at 228 and 326 K above ground, considerably higher than the 92 K of the upper state, $^2P_{3/2}$ of the 157.6 μm fine structure line of C^+.

The cooling by atomic oxygen is simple to model because atomic oxygen is a product of photodissociation and is therefore abundant only in gas with low A_V implying gas densities below the critical densities for collisional de-excitation, 6400 and 3400 cm^{-3} for the 63.2 and 145.6 μm lines, respectively (table 2.7 of Tielens 2005). At this density, we assume that the optically thin approximation applies. In this case, every collisional excitation to an upper state of the fine structure lines results in spontaneous emission that escapes the cloud and cools the gas:

$$\Lambda_O = n(O)n(H_2)(E_{21}C_{21} + E_{20}C_{20}) \text{ erg cm}^{-3} \text{ s}^{-1}, \quad \text{(A1)}$$

where the upward collision rates are

$$C_{21} = 1.4 \times 10^{-8} \frac{g_1}{g_2} C_{12} \exp(-E_{21}/kT)\sqrt{T} \text{ cm}^3 \text{ s}^{-1} \quad \text{(A2)}$$

$$C_{20} = 1.4 \times 10^{-8} \frac{g_0}{g_2} C_{02} \exp(-E_{20}/kT)\sqrt{T} \text{ cm}^3 \text{ s}^{-1}, \quad \text{(A3)}$$

the statistical weights are $g_2 = 5$, $g_1 = 3$, and $g_0 = 1$, and the transition energies are $E_{12}/k = 228$ K and $E_{02}/k = 326$ K.

APPENDIX B: CHEMISTRY

B1 Freeze-out

Molecules freeze on to dust grains, sticking when they collide. This process is easily modelled. We follow Keto & Caselli (2008) to calculate the collision time-scale. The time-scale for depletion on to dust may be estimated as (Rawlings et al. 1992)

$$\tau_{on} = (S_0 R_{dg} n(H_2) \sigma V_T)^{-1} \text{ s}. \quad \text{(B1)}$$

Here, S_0 is the sticking coefficient, with $S_0 = 1$ meaning that the colliding molecule always sticks to the dust in each collision; R_{dg} is the ratio of the number density of dust grains relative to molecular hydrogen; σ is the mean cross-section of the dust grains; and V_T is the relative velocity between the grains and the gas. If the grains have a power-law distribution of sizes with the number of grains of each size scaling as the -3.5 power of their radii (Mathis, Rumpl & Nordsieck 1977), then we can estimate their mean cross-section as,

$$\langle\sigma\rangle = \left(\int_{a_1}^{a_2} n(a)\,\mathrm{d}a\right)^{-1} \int_{a_1}^{a_2} n(a)\sigma(a)\,\mathrm{d}a, \tag{B2}$$

where a_1 and a_2 are the minimum and maximum grain sizes. If $a_1 = 0.005$ μm and $a_2 = 0.3$ μm, then $\langle\sigma\rangle = 3.4 \times 10^{-4}$ μm^2. Similarly, the ratio of the number densities of dust and gas may be estimated by computing the mean mass of a dust grain and assuming the standard gas-to-dust mass ratio of 100. If the density of the dust is 2 g cm^{-3}, then the ratio of number densities is $R_{dg} = 4 \times 10^{-10}$.

Consistent with Keto & Caselli (2008), our model has a slightly lower value for the grain cross-section, 1.4×10^{-21} cm^2, than Hollenbach et al. (2009), $\sigma_h = 2 \times 10^{-21}$ cm^2. Both values are per hydrogen nucleus ($2H_2 + H$). Because the ice forms and desorbs off the grain surfaces, larger values of the average cross-section result in fewer molecules in the gas phase. The actual properties of grains in cold clouds are somewhat uncertain.

The relative velocity due to thermal motion is

$$V_T = \left(\frac{8kT}{\pi\mu}\right)^{1/2}, \tag{B3}$$

where T is the temperature and μ the molecular weight. The freeze-out rate for species i is

$$f_i = \tau_{on}^{-1} n(H_2)\ \ \mathrm{cm}^{-3}\ \mathrm{s}^{-1}. \tag{B4}$$

B2 Gas-phase reactions

The neutral–neutral molecular and photodissociation reactions are from Tielens & Hollenbach (1985). The reaction rate k_1 for $O + H_2 \rightarrow OH + H$ is

$$k_1 = 3.1 \times 10^{-13}\,(T/300)^{2.7} \exp(-3150/T)\ \ \mathrm{cm}^3\ \mathrm{s}^{-1}. \tag{B5}$$

The reaction k_2 for $OH + H_2 \rightarrow H_2O + H$ is

$$k_2 = 2.0 \times 10^{-12}(T/300)^{1.57} \exp(-1736/T)\ \ \mathrm{cm}^3\ \mathrm{s}^{-1}. \tag{B6}$$

OH + H has a rate

$$5.3 \times 10^{-18}(T/300)^{-5.22} \exp(-90/T). \tag{B7}$$

All three of these reactions have an activation barrier and are irrelevant at temperatures below 300 K. The photodissociation rate for the destruction of OH and the formation of O is

$$P_1 = 3.5 \times 10^{-10} G_0 \exp(-1.7A_V)\ \ \mathrm{s}^{-1} \tag{B8}$$

and the rate for the destruction of H_2O and formation of OH is

$$P_2 = 5.9 \times 10^{-10} G_0 \exp(-1.7A_V)\ \ \mathrm{s}^{-1}. \tag{B9}$$

The unitless parameter $G_0 = 1$ corresponds to the average local interstellar radiation field in the FUV band (Habing 1968). A_V is the visual extinction.

B3 Desorption

The desorption rates are from Hollenbach et al. (2009). The total desorption rate includes thermal desorption, photodesorption, and desorption by cosmic rays. We use equation (2) from Hollenbach et al. (2009) for the rate for thermal desorption as

$$D_{Th} = 1.6 \times 10^{11} \left(\frac{E_i}{k}\right)^{1/2} \left(\frac{m_H}{m_i}\right)^{1/2} \exp\left(\frac{-E_i}{kT_{gr}}\right) \mathrm{s}^{-1}\ \mathrm{molecule}^{-1}, \tag{B10}$$

where E_i/k, the adsorption energy, is 800, 1300, and 5770 K for O, OH, and H_2O, respectively, and m_i/m_H is the weight of the species with respect to H. The thermal desorption rate for water is negligible at the temperatures (<15 K) of cold, dense clouds. For the cosmic ray desorption rate, we use equation (8) from Hollenbach et al. (2009). We include only the cosmic ray desorption rate for H_2O as

$$D_{CR} = 4.4 \times 10^{-17}\ \mathrm{molecule}^{-1}\ \mathrm{s}^{-1}. \tag{B11}$$

Both the thermal desorption rate and the cosmic ray desorption rate in units of molecule^{-1} s^{-1} are multiplied by the number of molecules on the surface of grains per molecule of H_2 which is $N_s f_s A_{gr} R_{dg}$, where $N_s = 10^{15}$ cm^{-2} is the number of desorption sites per cm^2 on the grain surface (Hollenbach et al. 2009), $f_s = 1$ is the fraction of the grain surface covered by ice, the average surface area of a grain is four times the grain cross-section, $A_{gr} = 4\sigma = 4 \times 3.4 \times 10^{-4}$ μm ^{2} (Keto & Caselli 2008), and the dust-to-gas ratio $R_{dg} = 4 \times 10^{-10}$ (Keto & Caselli 2008). The photodesorption rates are from equations (6) and (7) (Hollenbach et al. 2009),

$$D_{UV} = G_0 F_0 Y_i f_i\ \exp(-1.8A_V)\ \mathrm{s}^{-1}, \tag{B12}$$

where $F_0 = 10^8$ is the number of UV photons per Habing flux and $Y_i = 10^{-3}$ and 2×10^{-3} are the photodesorption yields per UV photon per second for the production of OH and H_2O, respectively, from table 1 of Hollenbach et al. (2009). We assume that all the ice is H_2O and follow Hollenbach et al. (2009) in assuming that the photodesorption of this water ice results in twice as much OH as H_2O in the gas phase.

The desorption of water ice does not result in the production of gas-phase oxygen, and we have no oxygen ice in our model. To provide a back reaction to the freeze-out of atomic oxygen, we arbitrarily assign a desorption rate equal to that of water. In regions of high extinction ($A_V > 4$), this results in a gas-phase abundance of atomic oxygen that is approximately the same as predicted by Hollenbach et al. (2009). This is <0.001 of the total oxygen and has no effect on the other abundances. In the outer part of the cloud where the UV flux is higher ($A_V < 4$), most of the atomic oxygen derives from photodissociation. Here, the UV desorption off grains is insignificant.

Additional desorption is caused by the UV photons emitted by hydrogen excitation by energetic electrons released in the ionization of hydrogen by cosmic rays. We follow Shen et al. (2004) and scale this process as 10^{-4} of one Habing flux, $G_0 = 1$, so that

$$D_{CRUV} = \alpha G_0 F_0 Y_i f_i\ \mathrm{s}^{-1} \tag{B13}$$

with $\alpha = 10^{-4}$.

B4 Equilibrium

In equilibrium, the rate equations in matrix form are

$$\begin{pmatrix} -(f_{\rm O}+k_1) & P_1 & 0 & 0 \\ k_1 & -(f_{\rm OH}+P_1) & P_2 & 0 \\ 0 & k_2 & -(f_{\rm H_2O}+P_2) & D_{\rm H_2O} \\ f_{\rm O} & f_{\rm OH} & f_{\rm H_2O} & -(D_{\rm OH}+D_{\rm H_2O}) \\ 1 & 1 & 1 & 1 \end{pmatrix} \times \begin{pmatrix} {\rm O} \\ {\rm OH} \\ {\rm H_2O} \\ {\rm ICE} \end{pmatrix} = \begin{pmatrix} 0 \\ 0 \\ 0 \\ 0 \\ 1 \end{pmatrix},$$

where the last row is the conservation equation for oxygen among all the species. As written, this system is overdetermined, but can be solved by dropping any one of the first four rows.

B5 H_2O ortho-to-para ratio

Since the ortho state of H_2O is 24 K above the para state, the O/P ratio in thermal equilibrium is very small at lower temperatures (equation 41; Hollenbach et al. 2009). However, when the water molecule is formed, created from OH on the grain surface for example, it is formed in the ratio of the available quantum states, ortho:para 3:1. The ortho and para states of H_2O equilibrate by collisions with H or H_2. If the chemical equilibrium time-scale is much shorter than the thermal equilibrium time-scale, the O/P ratio will not deviate much from 3:1. Observations generally show ratios close to 3:1 (van Dishoeck et al. 2013).

We have not found previous research on the equilibration of H_2O, but an appreciation of the time-scale can be estimated from previous research on the equilibration of the ortho and para states of molecular hydrogen. The dissociation energies of H–H and OH–H are not too different nor the collisional cross-sections of the molecules. Conrath & Gierasch (1984) and Fouchet, Lellouch & Feuchtgruber (2003) suggest that three processes for the equilibration of the ortho and para states of H_2 are: (1) gas-phase H exchange, (2) gas-phase paramagnetic conversion with H_2, and (3) H exchange on a surface. We assume that these same processes are applicable to the water. The rates for these processes scale with the gas density through the collision rate and scale as the inverse exponential of the temperature. Scaling the rates for H_2 from the conditions in the atmosphere of Jupiter to rarefied, cold gas of the ISM (10 K and 10^6 cm^{-3}), the time-scales for these processes are all >1 Gyr.

In contrast, the chemical time-scale is very much shorter (Fig. 5) throughout the cloud. In this model, water is dissociated in the gas phase by photodissociation and also coming off the grain surfaces by photodesorption in which gas-phase OH is produced twice as often as gas-phase H_2O. The equilibrium comparison between ortho–para equilibration and chemistry may not be needed because the equilibration time-scale exceeds the expected lifetimes of the cold, dense clouds.

This paper has been typeset from a TEX/LATEX file prepared by the author.